Electronic Supplementary Material (ESI) for Materials Chemistry Frontiers.

Supporting Information

Switchable photon and phonon emission properties of an atomically precise Ag_{14} core-based two-dimensional silver cluster-assembled material

*Anish Kumar Das,‡[a] Sourav Biswas,‡[a] Anjali Thomas,[b] Souradip Paul,[b] Akhil S. Nair,[c] Biswarup Pathak,[c] M. Suheshkumar Singh,[b] Sukhendu Mandal [a] **

[a] *School of Chemistry, Indian Institute of Science Education and Research Thiruvananthapuram, Kerala 69551, India. E-mail: sukhendu@iisertvm.ac.in*

[b] *Biomedical Instrumentation and Imaging Laboratory, School of Physics, Indian Institute of Science Education and Research Thiruvananthapuram, Kerala 695551, India.*

[c] *Department of Chemistry, Indian Institute of Technology, Indore, Madhya Pradesh 453552, India.*

‡ These authors contributed equally to this work.

Table of contents

Experimental Section

Materials

All chemicals were purchased commercially and used without prior purification. Silver nitrate ($AgNO_3$), tert butylthiol (HS^tBu), silver trifluoroacetate (CF_3COOAg), phenyl phosphonic acid, and 4,4'-azopyridine were procured from Sigma-Aldrich. HPLC grade solvents- methanol, ethanol, acetonitrile, chloroform, and triethylamine (Et_3N) were purchased from Spectrochem. Milli-Q water was used in all experiments. All glassware was thoroughly cleaned with aqua regia (HCl: HNO_3= 3:1, v:v), rinsed with copious pure water.

Synthesis of two-dimensional Ag_{14} cluster-assembled material

Crystal 1 was synthesized by a facile one-pot synthetic approach. 0.1 mmol of AgS^tBu and 0.1 mmol of CF_3COOAg were sequentially added into the 6 ml of a solvent mixture of E/A (1:1) and stirred up to form a colorless clear solution. Subsequently, 0.13 mmol of phenyl phosphonic acid and 0.13 mmol of 4,4'-azopyridine were sequentially added into both solution mixtures and kept stirring for another 15 min at room temperature. A yellowish-brown precipitate was formed and that was separated by centrifugation. Then the final clear solution was kept at room temperature in a dark environment for 3 days and crystals were obtained by slow evaporation of the solvent (Yield: 58 % on the basis of Ag). The precursor, AgS^tBu complex was synthesized by treating the equivalent amount of $AgNO_3$ and HS^tBu with Et_3N, as reported in the literature.[1] The use of multi-dentate phenyl phosphonic acid is crucial here because of its H-bond donating ability, and we observed that without adding it, we can't get the desired product.

In the case of the E/C mixture, we just replaced the solvent medium in this protocol to synthesize **crystal 1a**. After adding AgS^tBu and CF_3COOAg in that solution mixture it turns greenish-yellow colored clear solution instead of this all other observations are the same as the E/A mixture (Yield: 51 % on the basis of Ag).

X-ray Crystallography

The single-crystal X-ray diffraction data for cluster-assembled material was collected on the Bruker Axs Kappa Apex II SC-XRD diffractometer with CCD detector using monochromated MoK_α radiation (λ= 0.71073 Å). The crystal structure was solved by SHELXT 201449 and refined by the full-matrix least-squares method using SHELXL 201850 present in the program

suite WinGX (version 2014.1).[2-4] All non-hydrogen atoms were refined anisotropically and hydrogen atoms were (positioned geometrically) refined isotropically using an olex2.[5]

Computational Details

DFT calculations were done using Gaussian 09 D.01 program.[6] B3LYP functional with Pople's 6–31G* basis set was used for non-metal elements and LANL2DZ-ECP (effective core potential) was employed for silver atoms, respectively.[7] Conductor-like polarizable continuum model (CPCM) with acetonitrile and chloroform were employed for solvent calculations.[8] The TD-DFT calculations considered 300 singlet-to-singlet excitation energies. The calculations were carried out for the molecular unit of the silver cluster-assembled material (CAM).

The stability calculations of bulk Ag CAM with periodic boundary conditions were carried out using Vienna Ab-Initio Simulation Package (VASP) employing optPBE van der Waals functional.[9] A similar calculation without van der Waals consideration was also carried out using Generalized gradient approximation of Perdew–Burke–Ernzerhof (PBE) functional for identifying the role of non-covalent interactions in determining the relative stability of the two crystal structures.[10, 11] Projector augmented wave (PAW) method was used for treating ion-electron interactions.[12, 13] The ionic relaxations have been carried out using a conjugate gradient algorithm with convergence criteria of 10^{-4} eV for minimum energy and 0.05 eV $Å^{-1}$ for Hellmann-Feynman forces on atoms. Due to the large size of the unit cells of the compounds, the Brillouin zone was sampled at the Gamma point (1×1×1).

Instrumentation

UV-vis spectroscopy was carried out on a UV-3800 SHIMADZU UV−vis/NIR spectrometer using a 3.5 ml cuvette. Emission measurements were performed using a Fluorolog-3 spectrofluorimeter from Horiba Jobin Yvon. The relative quantum yields were determined by the best match of the excitation wavelength of a well-known chromophore such as Perylene with the crystals and the excitation was fixed at 410 nm. The concentration of the solutions was fixed by adjusting the absorption 0.05 OD and measured the quantum yield at room temperature. XPS measurements have been done using the Omicron Nanotech instrument (MgK_α radiation at 1253.6 eV). All binding energies were referenced to the neutral C 1s peak at 284.8 eV. IR spectra (with the spectral resolution of 4 cm^{-1}) were collected on a Shimadzu IRPrestige–21 FTIR spectrometer by using the KBr pellet method. Solution-state FT-IR spectra were recorded by a Bruker-Alpha (ATR-ZnSe) instrument. Bruker Avance III, 500 MHz, NMR

was used for the ^{1}H and ^{19}F NMR studies. PXRD data were collected employing an X'pert PRO (PANalytics) powder diffractometer equipped with a Cu Kα (λ = 1.5405 Å) radiation source. The TGA was performed on SDT Q600 (Shimadzu) analyzer from room temperature to 600 ^{o}C at a heating rate of 10 ^{o}C min^{-1} under N_2 atmosphere. Emission lifetimes were measured using a picosecond time-correlated single-photon counting system (model Horiba Jobin Yvon-IBH). Solutions were excited at 475 nm using a pulsed diode laser. The fluorescent decay curve was fitted with a monoexponential decay fit.

PA-images were recorded for **crystal 1** and **1a** in E/A and E/C solvent mixture and the solutions were taken inside two different transparent tubes with inner diameter 0.28 mm and kept in the sample holder of the transmission conFig.d home-built acoustic resolution photoacoustic microscopy (AR-PAM) imaging system.[14] Each sample was illuminated with an optical beam of 2.3 mm diameter, and a tuneable 100 Hz pulse repetition frequency of a 6 nsec pulse width (SpitLight OPO Evo 150–532, Innolas Lasers, Krailling, Germany), coupled by an optical fibre. The energy and wavelength of the laser were set as 10 mJ and 450 nm, respectively. The induced PA signal was collected by a tightly focusing 30 MHz (focal spot size 154 μm and focal length 19.10 mm) ultrasound transducer (V375-SU, Olympus, Shinjuku City, Tokyo, Japan). The detected signal was then amplified using an amplifier (Part No.: VCA2615EVM, Texas Instruments, Dallas, Texas, USA), sampled using a data acquisition card (Part No.: 779745-02, NI PCI-5114, 250 MS/s, National Instruments, Austin, Texas, USA) and saved to the system for further processing. To produce the 3D data, raster scanning of the transducer with step-size 100 μm was utilized with a high precession translation stage (Newmark NSC-G series, Newmark Systems Inc., Rancho Santa Margarita, CA, USA). From these data MAP (Maximum Amplitude Projection) images along depth were produced with MATLAB for comparison and analysis.

To enhance PA signal strength, we adopted our reported optical pre-illumination technique in which CW-optical beam from a laser source (NPL52B, Thorlabs, Newton, New Jersey, USA; wavelength, 520 nm, power, 40 mW) – in addition to pulse-laser beam adopted for generating of PA waves – was employed to illuminate the samples by intersecting the pulse-laser beam and CW-beam at a pre-specified section.[14] Continuously switched on CW-laser retain the temperature throughout the experiment and we call this process pre-illumination. Here we have used a pulsed laser at 650 nm for imaging so that the change in PA signal with temperature will be much more visible.

Table S1a. Crystal data and structure refinement parameters for **Crystal 1**

Identification code	**Crystal 1**
CCDC number	2093651
Empirical formula	$C_{34}\ H_{53}\ Ag_7\ F_6\ N_4\ O_4\ S_5$
Formula weight	1611.19
Temperature	150 (2) K
Wavelength	0.71073 Å
Crystal system	Monoclinic
Space group	*C2/c*
Unit cell dimensions	a = 23.087(3) Å; b = 14.5454(17) Å, c = 30.330(4) Å; α = 90°; β = 102.868(5) °; γ = 90°
Volume	9929(2) $Å^3$
Z	8
Density (calculated)	2.156 mg/m^3
Absorption coefficient	2.975 mm^{-1}
F(000)	6240
Crystal size	0.075 x 0.035 x 0.025 mm^3
Theta range for data collection	1.377 to 28.374 °.
Limiting indices	-30<=h<=30, -19<=k<=19, -40<=l<=40
Reflections collected	69651
Independent reflections	12386 [R(int) = 0.2494]
Completeness to theta = 25.242 °	99.9 %
Refinement method	Full-matrix-block least-squares on F^2
Data / restraints / parameters	12386 / 0 / 551
Goodness-of-fit on F^2	0.930
Final R indices [I > 2sigma(I)]	R_1 = 0.0713, wR_2 = 0.1494
R indices (all data)	R_1 = 0.1930, wR_2 = 0.2154
Largest diff. peak and hole	1.630 and -1.930 e. $Å^{-3}$

Table S1b. Crystal data and structure refinement parameters for **Crystal 1a**

Identification code	**Crystal 1a**
CCDC number	2093652
Empirical formula	C_{34} H_{53} Ag_7 F_6 N_4 O_4 S_5
Formula weight	1611.19
Temperature	150 (2) K
Wavelength	0.71073 Å
Crystal system	Monoclinic
Space group	*C2/c*
Unit cell dimensions	a = 23.0645(19) Å; b = 14.5322(12) Å, c = 30.379(3) Å; α = 90°; β = 102.842(3) °; γ = 90°
Volume	9927.6(14) $Å^3$
Z	8
Density (calculated)	2.156 mg/m^3
Absorption coefficient	2.975 mm^{-1}
F(000)	6240
Crystal size	0.085 x 0.057 x 0.035 mm^3
Theta range for data collection	1.375 to 28.417 °.
Limiting indices	-30<=h<=30, -19<=k<=19, -40<=l<=40
Reflections collected	87500
Independent reflections	12396 [R(int) = 0.1488]
Completeness to theta = 25.242 °	99.9 %
Refinement method	Full-matrix-block least-squares on F^2
Data / restraints / parameters	12396 / 0 / 556
Goodness-of-fit on F^2	1.005
Final R indices [I > 2sigma(I)]	R_1 = 0.0544, wR_2 = 0.1139
R indices (all data)	R_1 = 0.1196, wR_2 = 0.1437
Largest diff. peak and hole	1.269 and -1.588 e. $Å^{-3}$

Table S2. Bond distances of **crystal 1**.

Ag_{14} CAM	**Bond distances (Å)**
Ag1-Ag2	2.948
Ag1-Ag3	3.016
Ag1-Ag6	3.189
Ag2-Ag4	2.948
Ag4-Ag5	2.934
Ag5-Ag1	3.036
Ag5-Ag7	3.098
Ag1-S1 (μ_4)	2.405
Ag2-S1 (μ_4)	2.444
Ag3-S1 (μ_4)	2.695
Ag4-S1 (μ_4)	2.962
Ag3-S2 (μ_3)	2.458
Ag6-S2 (μ_3)	2.486
Ag7-S2 (μ_3)	2.413
Ag2-S3 (μ_3)	2.379
Ag4-S3 (μ_3)	2.491
Ag7-S3 (μ_3)	2.655
Ag1-S4 (μ_3)	2.398
Ag5-S4 (μ_3)	2.445
Ag6-S4 (μ_3)	2.554
Ag4-S5 (μ_3)	2.551
Ag5-S5 (μ_3)	2.503
Ag7-S5 (μ_3)	2.484
Ag5-O1	2.423
Ag4-O2	2.302
Ag6-O3	2.433
Ag3-O4	2.450

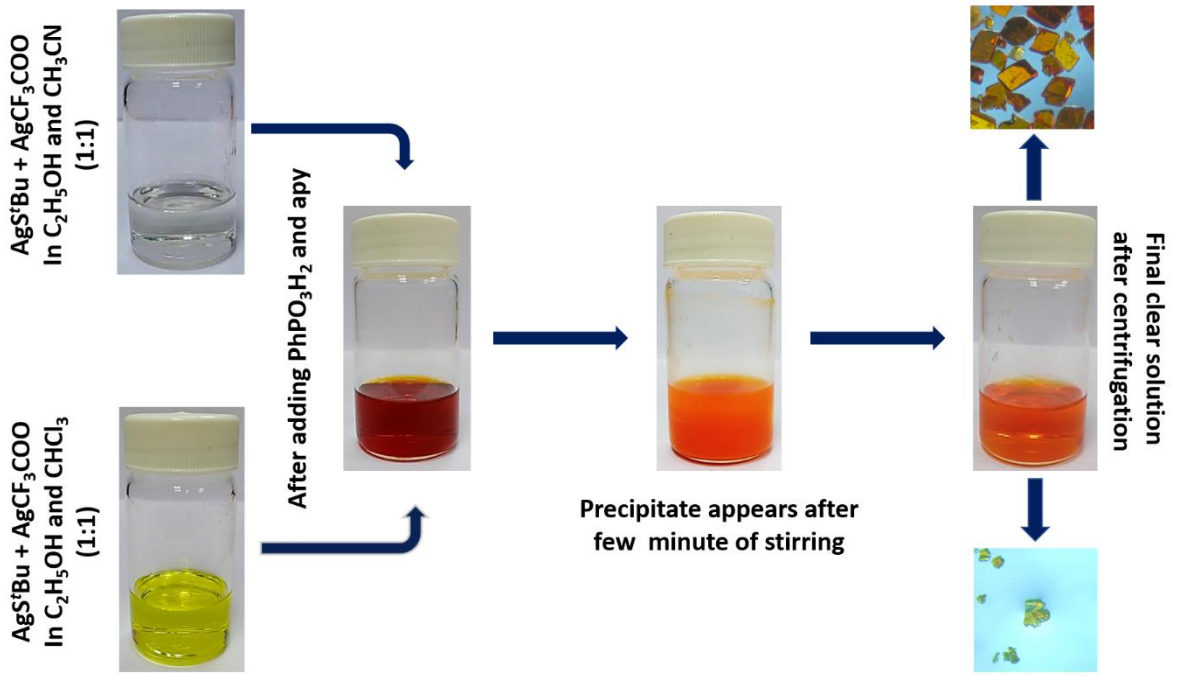

AgS^{t}Bu	AgCF$_3$COO	4,4'-azopyridine	Results
0.1 mmol	0.1 mmol	0.065 mmol	Crystals with impurity
0.05 mmol	0.05 mmol	0.13 mmol	No crystals
0.05 mmol	0.1 mmol	0.13 mmol	Powder
0.1 mmol	0.05 mmol	0.13 mmol	Crystals with impurity
0.1 mmol	0.1 mmol	0.13	Pure crystals

Fig. S1 Synthetic route of $Ag_{14}(S^tBu)_{10}(CF_3COO)_4(apy)_2$ in ethanol/acetonitrile (**crystal 1**) and ethanol/chloroform mixture (**crystal 1a**), below optimization table of the reagents. This optimization table we have followed in E/A (3 ml/3 ml) and in E/C (3 ml/3 ml) solvent mixture separately keeping fixed the amount of the phenyl phosphonic acid as it is not bonded with the crystals.

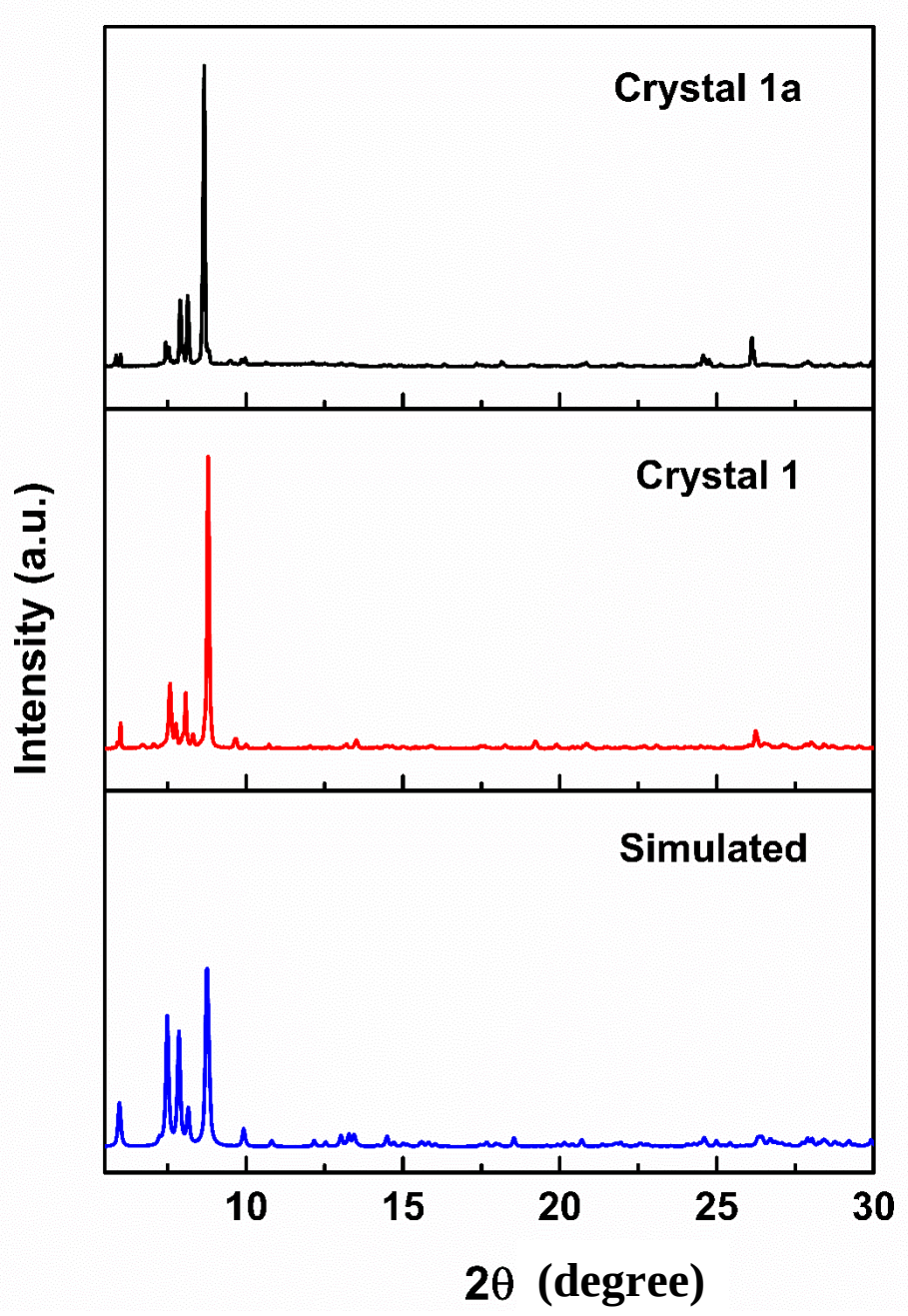

Fig. S2 Simulated and experimental PXRD patterns of **crystal 1** and **crystal 1a.**

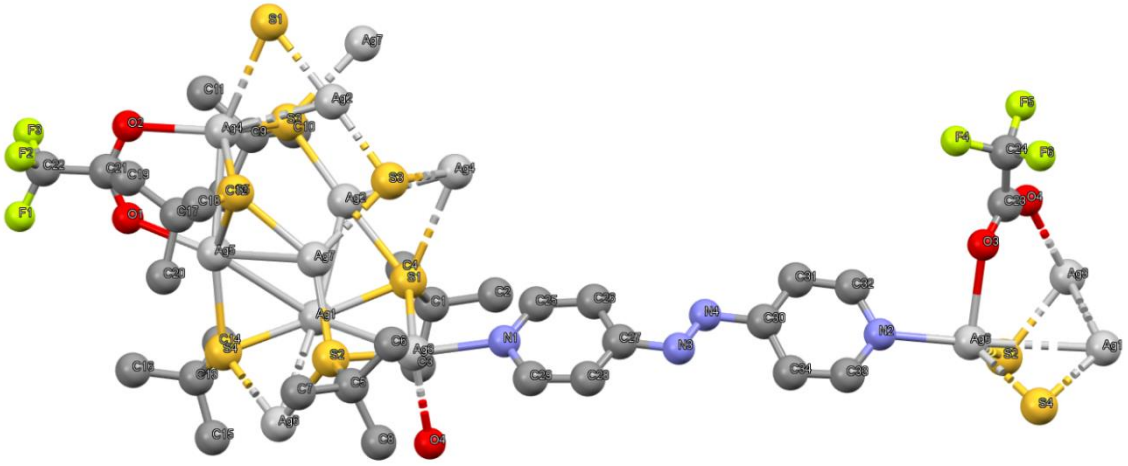

Fig. S3 Asymmetric unit of **crystal 1**.

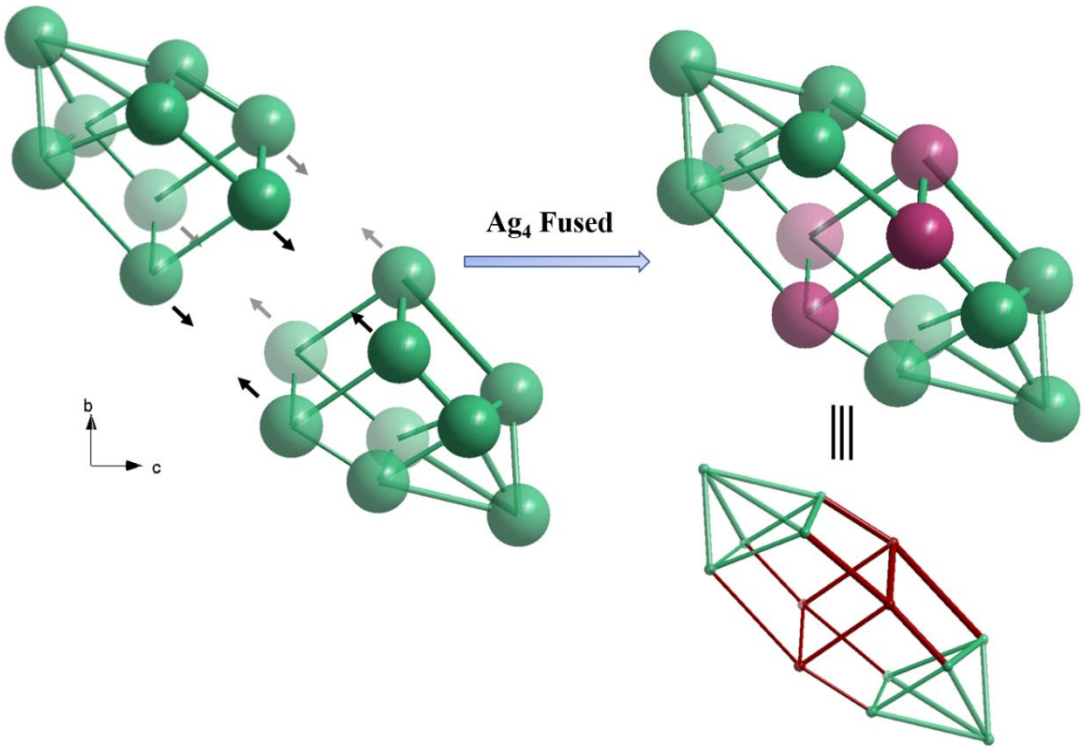

Fig. S4 Schematic formation of ortho-bielongated square pyramid core geometry by face fusion of two distorted elongated square pyramid.

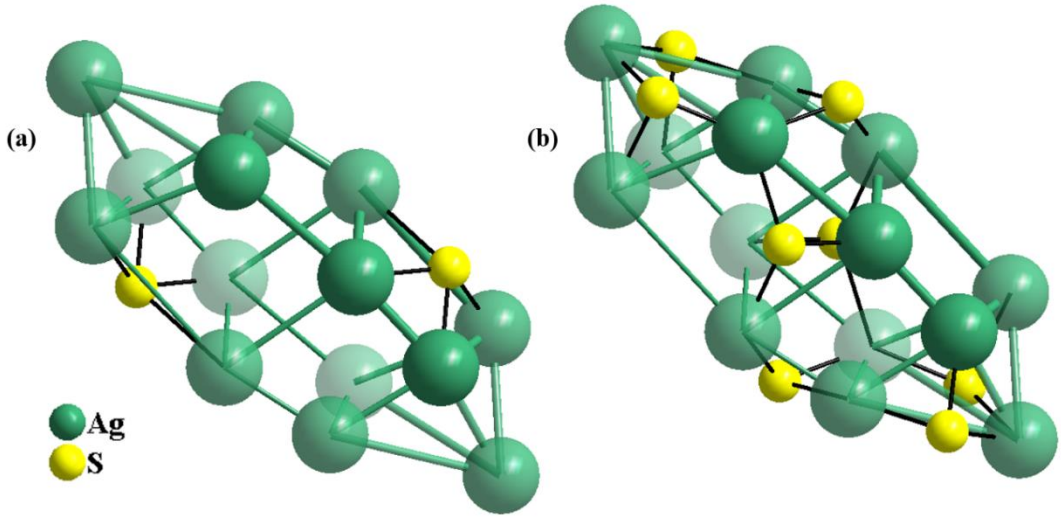

Fig. S5 Arrangement of μ_4 and μ_3 S with the Ag_{14} core.

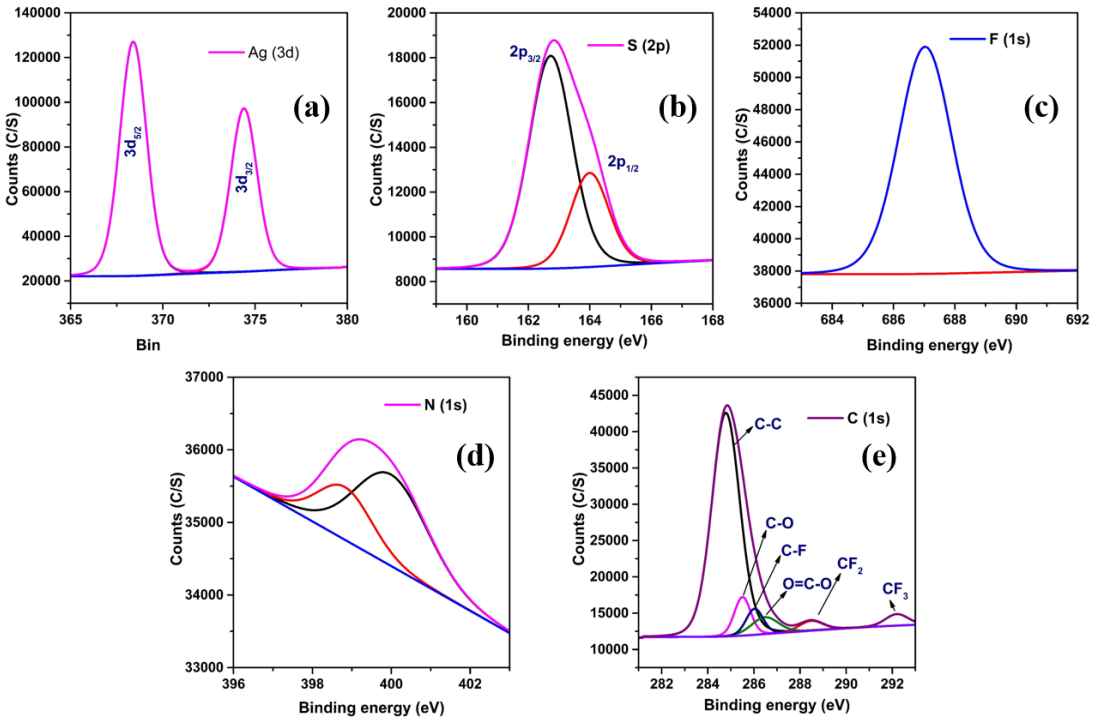

Fig. S6 The deconvolution of XPS data of (a) $3d_{5/2}$ and $3d_{3/2}$ for Ag ; (b) $2p_{3/2}$ and $2p_{1/2}$ for S atom, (c) 1*s* for F atom, (d) 1*s* for N atom and (e) 1*s* for C atom of **crystal 1**.

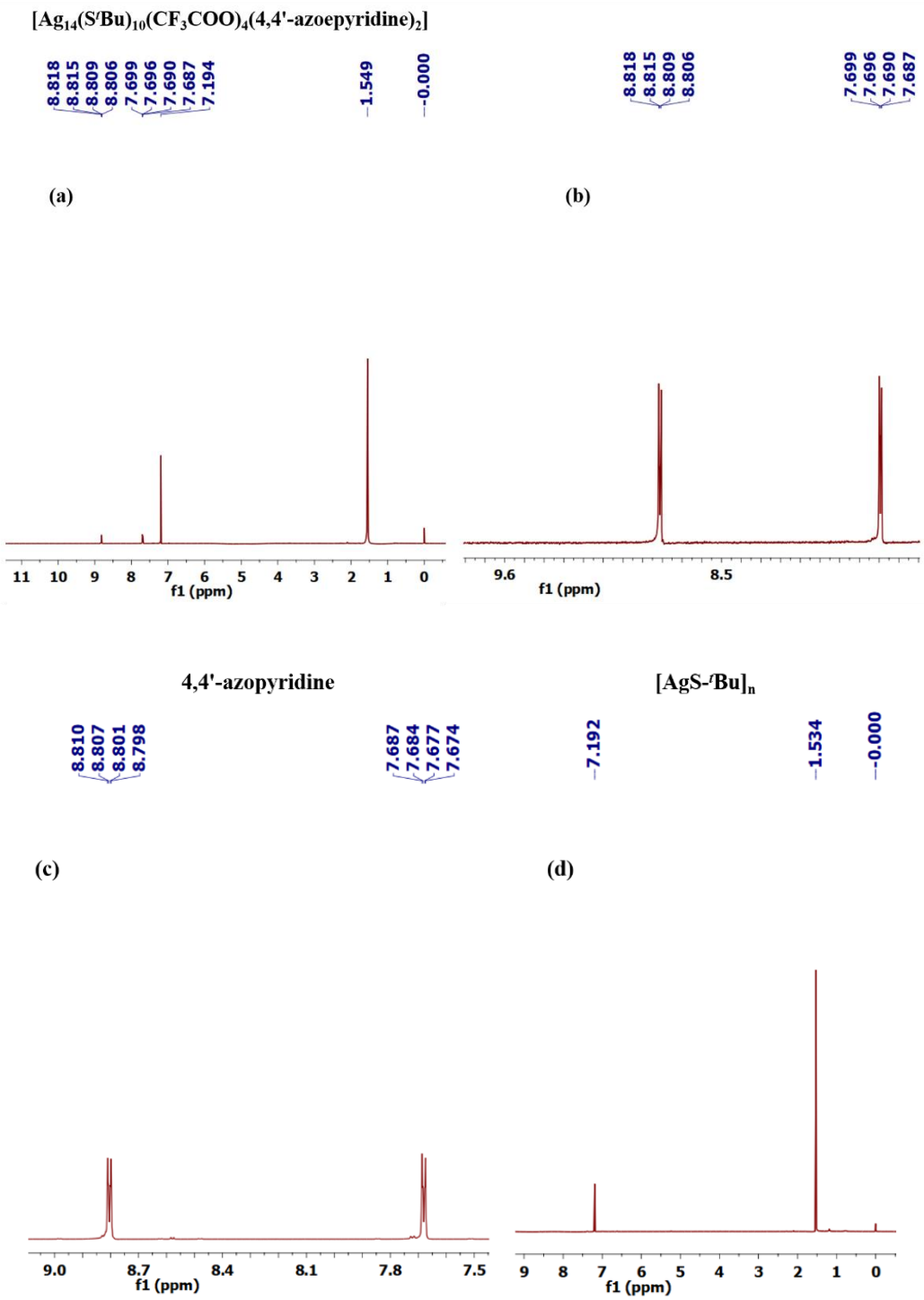

Fig. S7 ^{1}H NMR in $CDCl_3$ of (a) **crystal 1**, (b) aromatic region of **crystal 1**, (c) 4,4'-azopyridine, and (d) $[AgS\text{-}^{t}Bu]_n$.

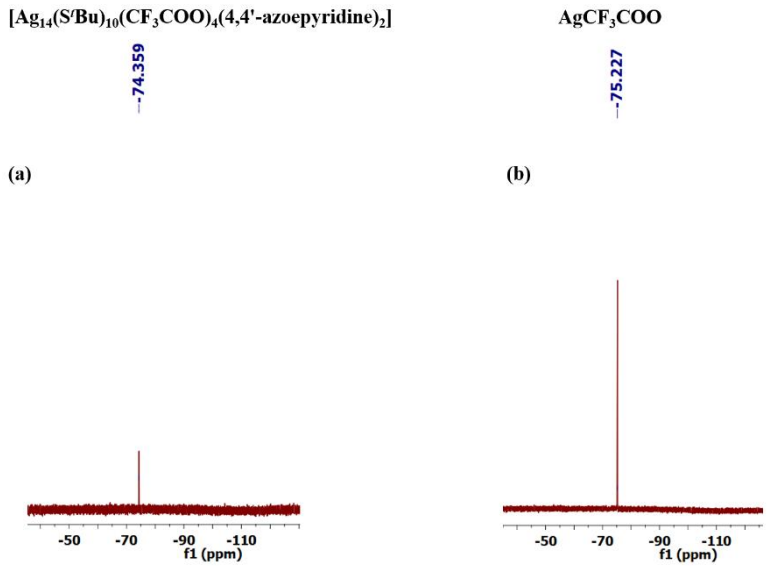

Fig. S8 ^{19}F NMR in $CDCl_3$ of (a) **crystal 1** and (b) $AgCF_3COO$.

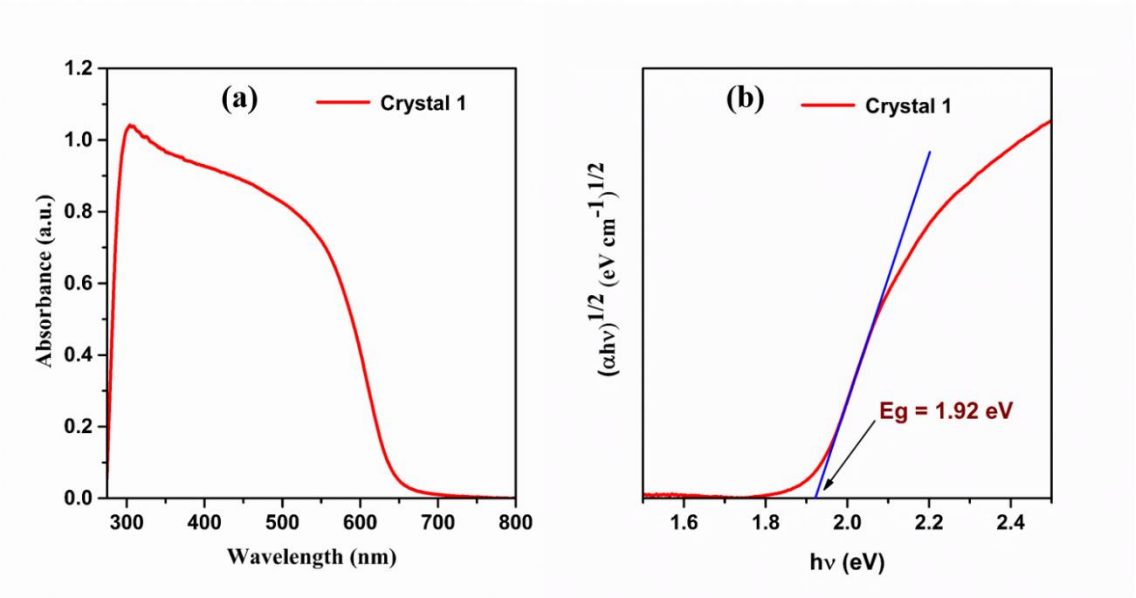

Fig. S9 (a) Solid-state UV-vis absorbance of **crystal 1** and (b) its characteristic band gap energy**.**

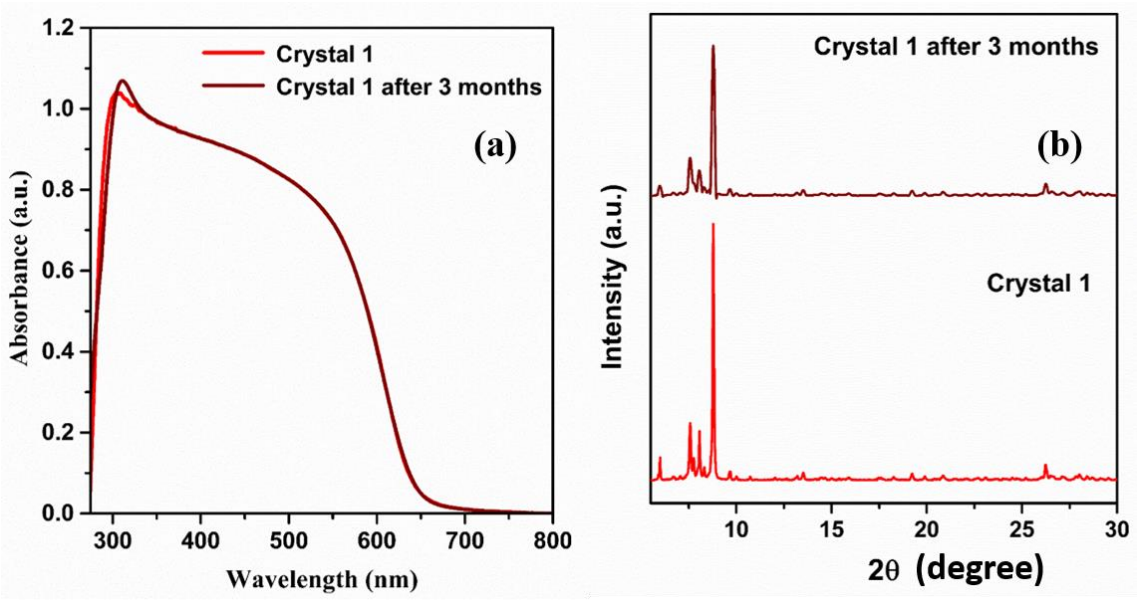

Fig. S10 (a) Solid-state UV-vis absorbance and (b) PXRD of **crystal 1** in day one of synthesis and after 90 days of synthesis.

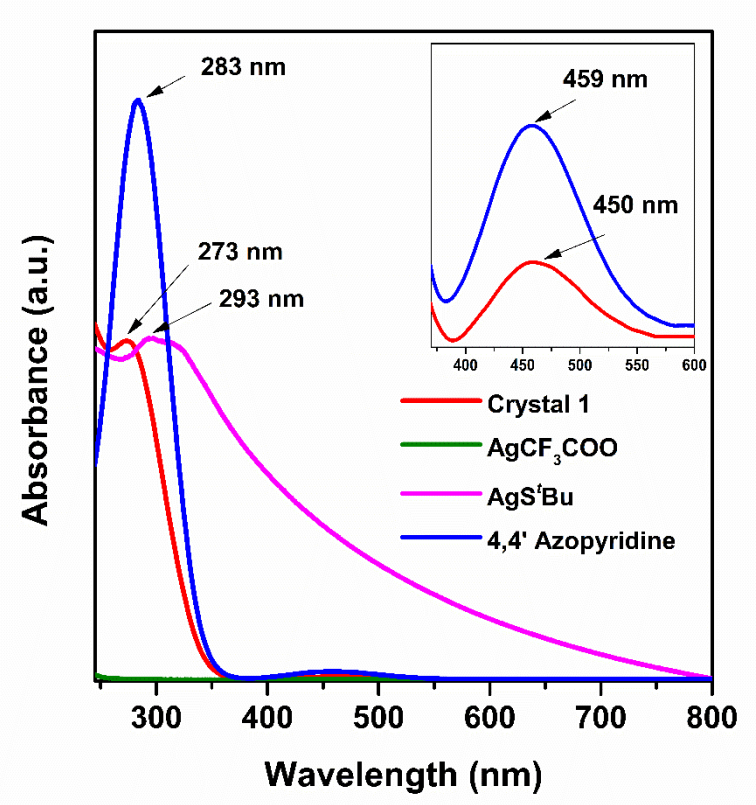

Fig. S11 UV-vis absorbance of **crystal 1** and the precursors in E/A medium.

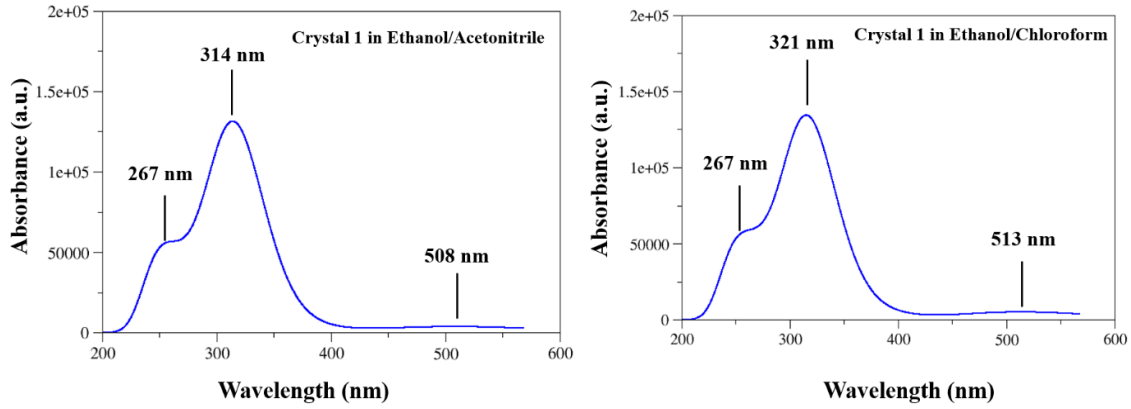

Fig. S12 Theoretically simulated absorbance spectra for the molecular unit of the crystals using time-dependent density functional theory (TDDFT) calculations by the Gaussian 09 program.

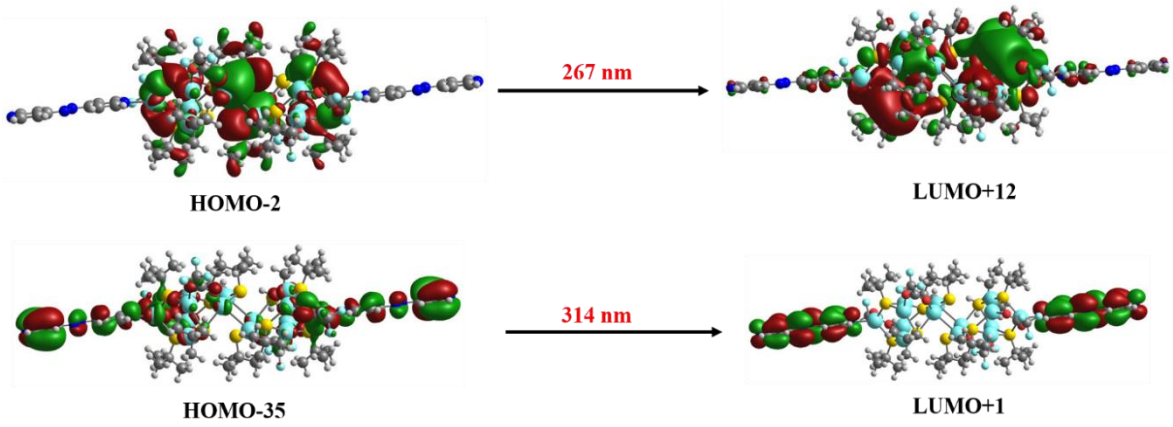

Fig. S13 Molecular Orbitals involved in optical transitions of **crystal 1** in ethanol/acetonitrile solvent mixture. Colour code: Ag (large Cyan), S (yellow), O (red), N (blue), F (small Cyan), C (gray), H (white).

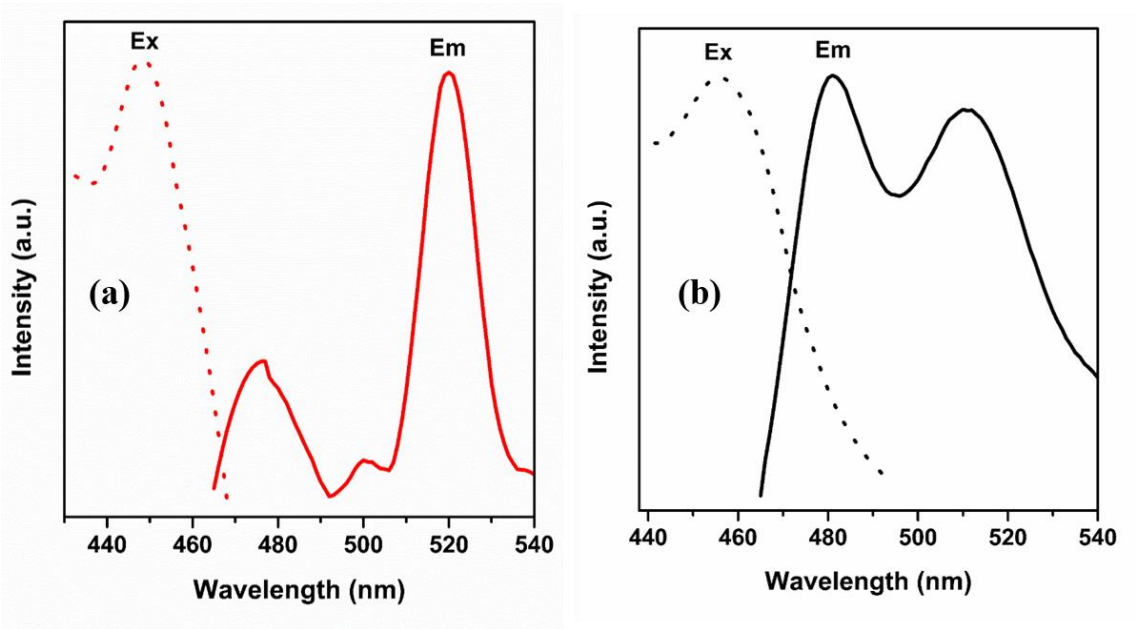

Fig. S14 PL excitation and emission of **crystal 1** in (a) E/A and (b) E/C medium.

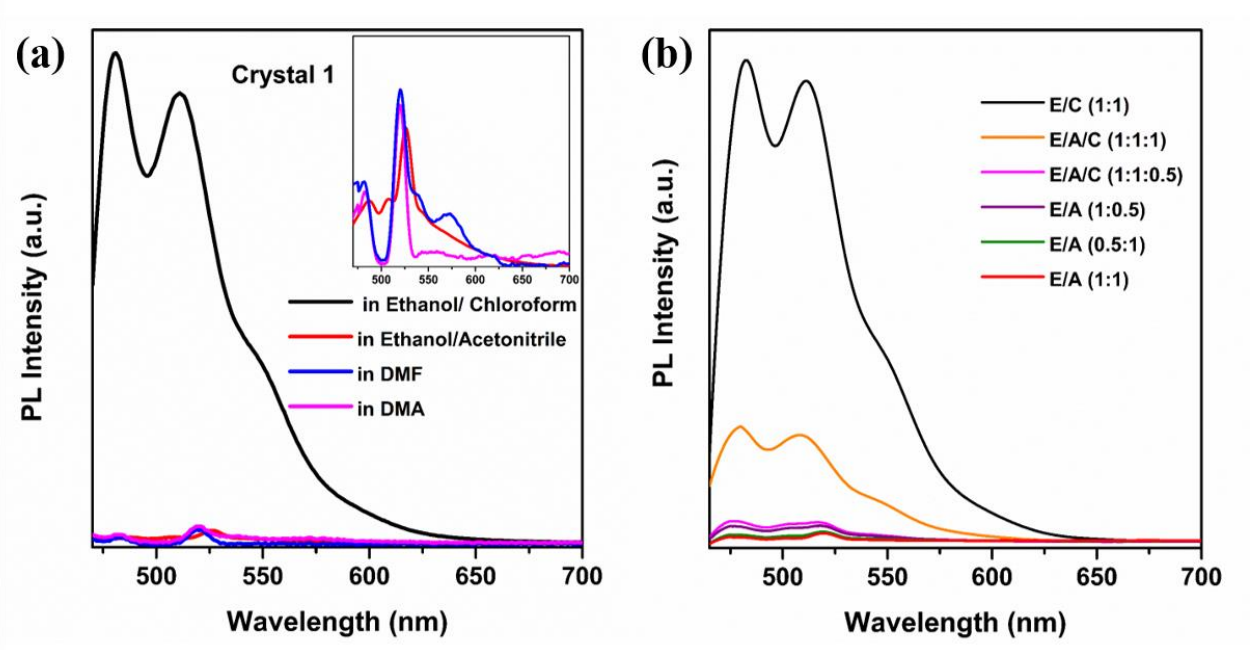

Fig. S15 (a) PL of **crystal 1** dissolving in different solvents and (b) dissolving in different ratios of the ethanol/acetonitrile (E/A), ethanol/chloroform (E/C), and mix of three solvents ethanol/acetonitrile/ chloroform (E/A/C).

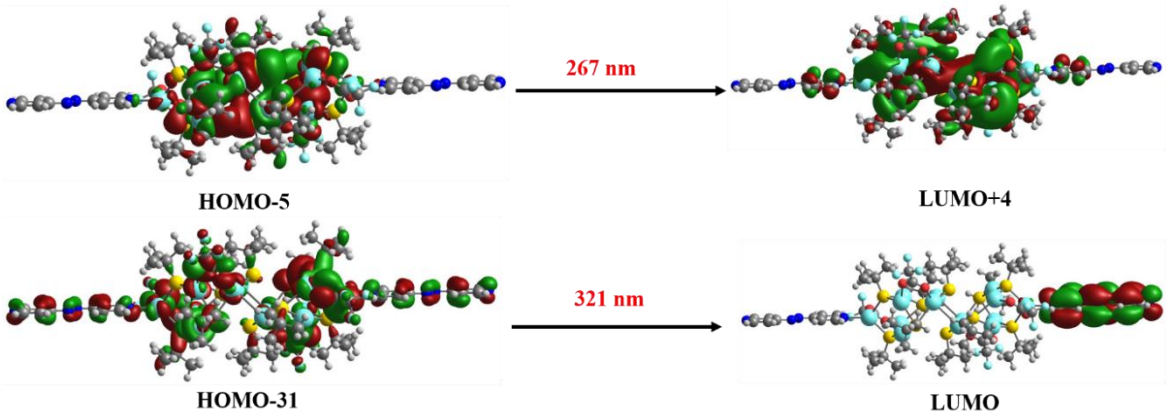

Fig. S16 Molecular Orbitals involved in optical transitions of **crystal 1** in ethanol/chloroform solvent mixture. Colour code: Ag (large Cyan), S (yellow), O (red), N (blue), F (small Cyan), C (gray), H (white).

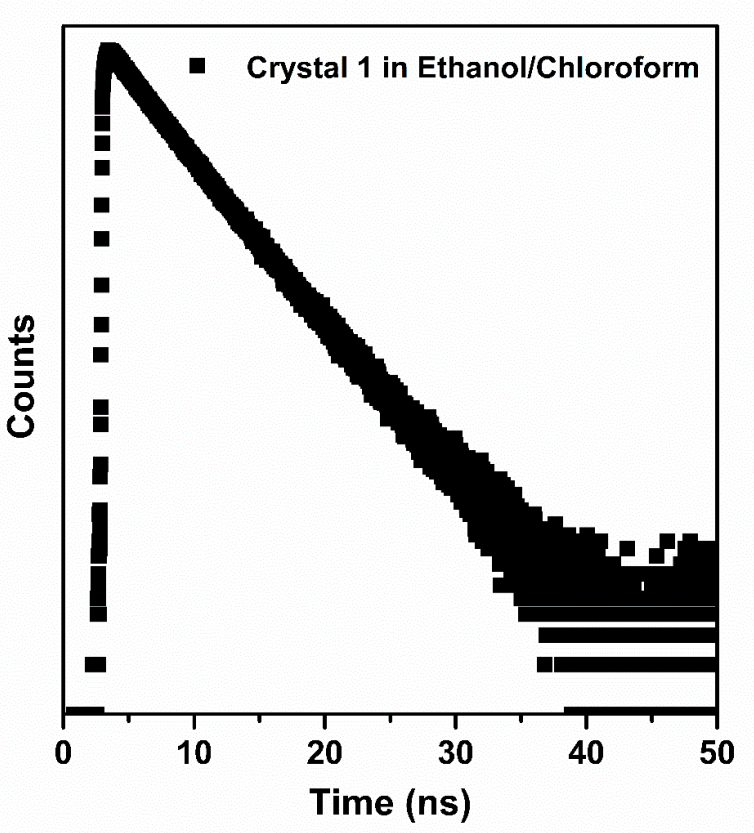

Fig. S17 TCSPC trajectories of **crystal 1** in ethanol/chloroform mixture.

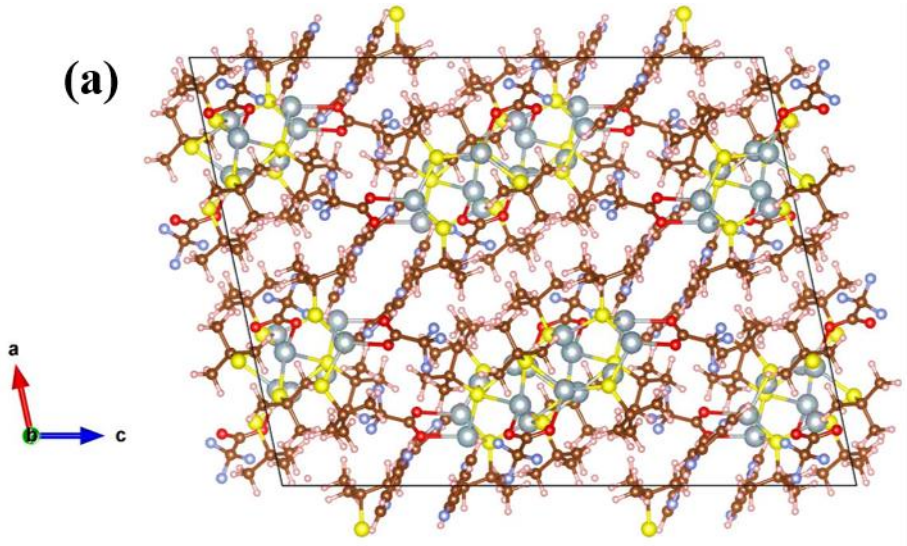

DFT optimized energy with optPBE vdW method: -4178.788 eV

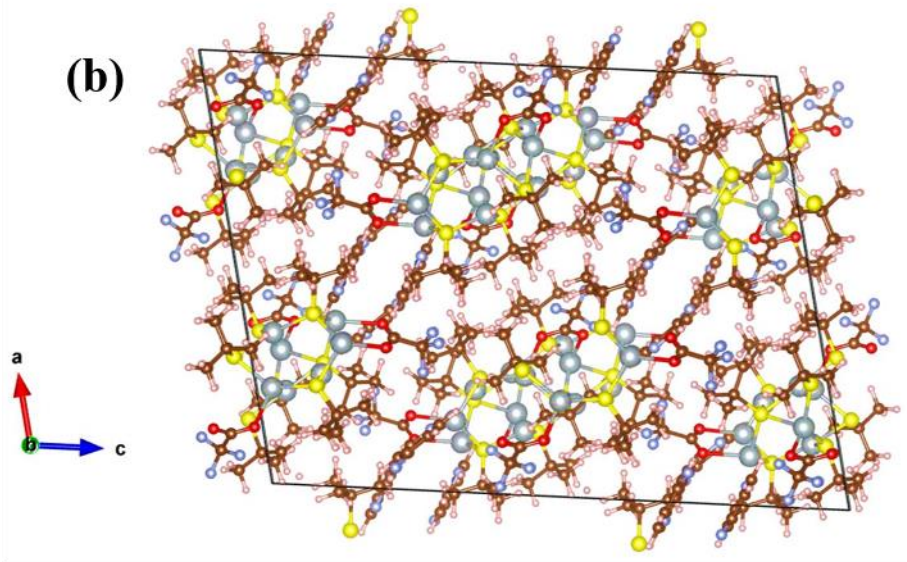

DFT optimized energy with optPBE vdW method: -4178.837 eV

Fig. S18 Relative stability of (a) **crystal 1** and (b) **crystal 1a** obtained from DFT calculations.

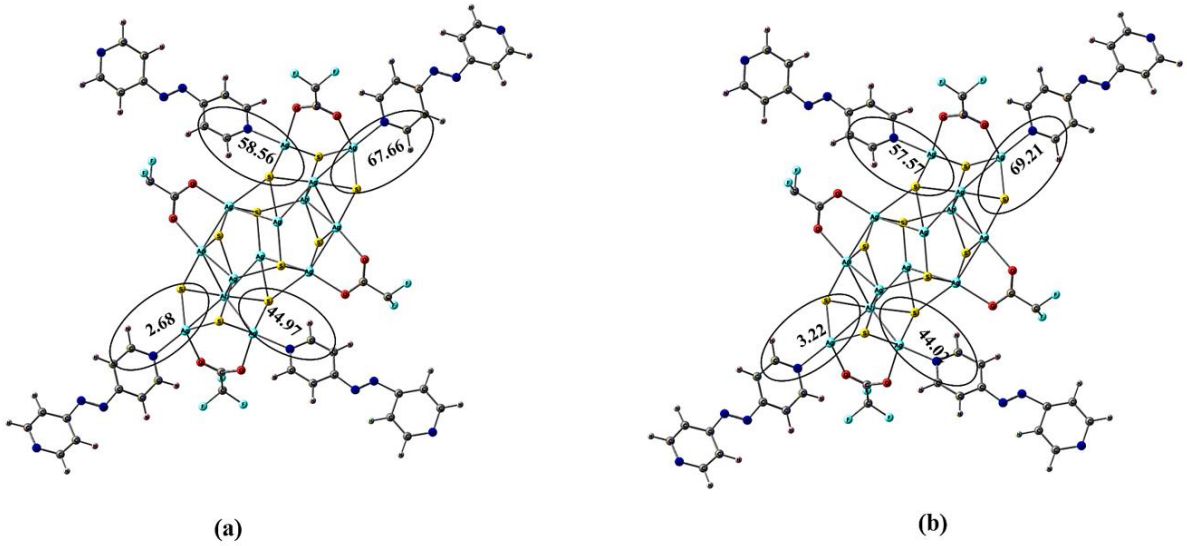

Fig. S19 Dihedral angle between linker and core in (a) **crystal 1** and (b) **crystal 1a**. The methyl groups are omitted for clarity.

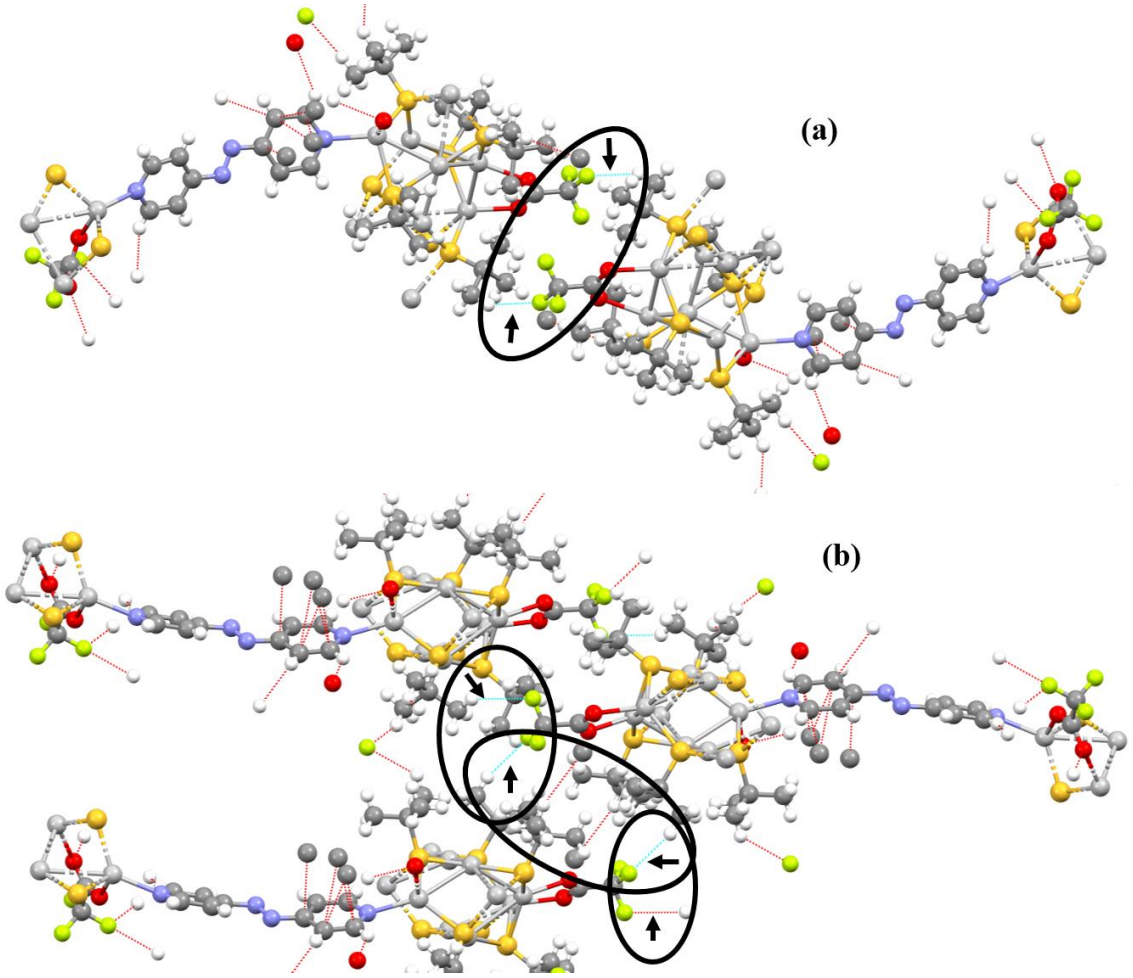

For crystal 1

Nr	Typ	Res	Donor	---	H....Acceptor	[ARU]	D - H	H...A	D...A	D - H...A	A..H..A*	A'..H..A"
1	Intra	1	C3	--H01H	..O4	[ ]	0.96	2.54	3.45(2)	158		
2		1	C29	--H25	..O4	[2655.01]	0.93	2.58	3.280(16)	133		
3	Intra	1	C25	--H28	..O2	[ ]	0.93	2.54	3.200(15)	128		

For crystal 1a

Nr	Typ	Res	Donor	---	H....Acceptor	[ARU]	D - H	H...A	D...A	D - H...A	A..H..A*	A'..H..A"
1	Intra	1	C3	--H3C	..O4	[ ]	0.96	2.55	3.453(13)	156		
2		1	C6	--H6B	..F4	[2555.01]	0.96	2.54	3.424(11)	153		
3	Intra	1	C25	--H25	..O2	[ ]	0.93	2.54	3.199(11)	128		
4		1	C29	--H29	..O4	[2555.01]	0.93	2.55	3.255(10)	132		

Fig. S20 Inter-cluster C-H···F interaction of (a) **crystal 1** and (b) **crystal 1a** and corresponding crystallographic C-H···F interaction.

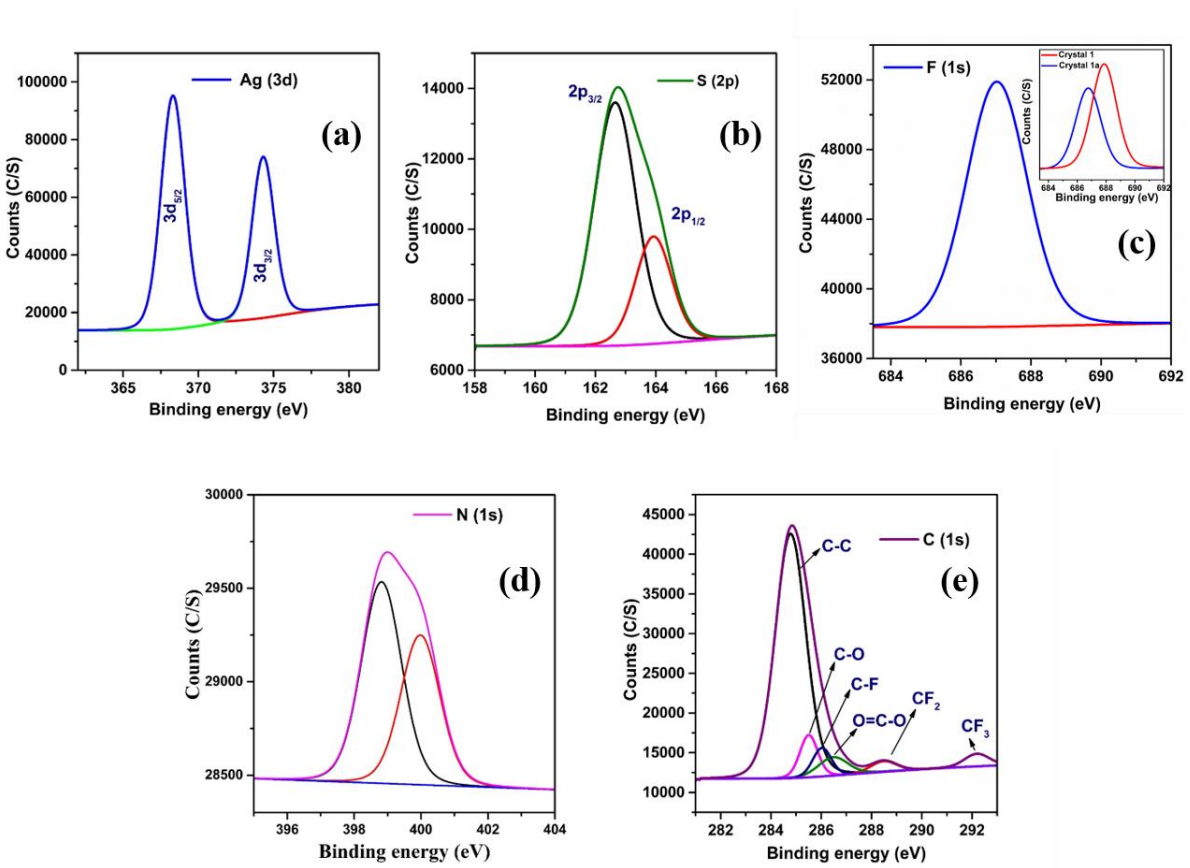

Fig. S21 The deconvolution of XPS data of (a) $3d_{5/2}$ and $3d_{3/2}$ for Ag, (b) $2p_{3/2}$ and $2p_{1/2}$ for S atom, (c) 1*s* for F atom inset showing the difference of binding energy of both crystals, (d) 1*s* for N atom and (e) 1*s* for C atom of **crystal 1a**.

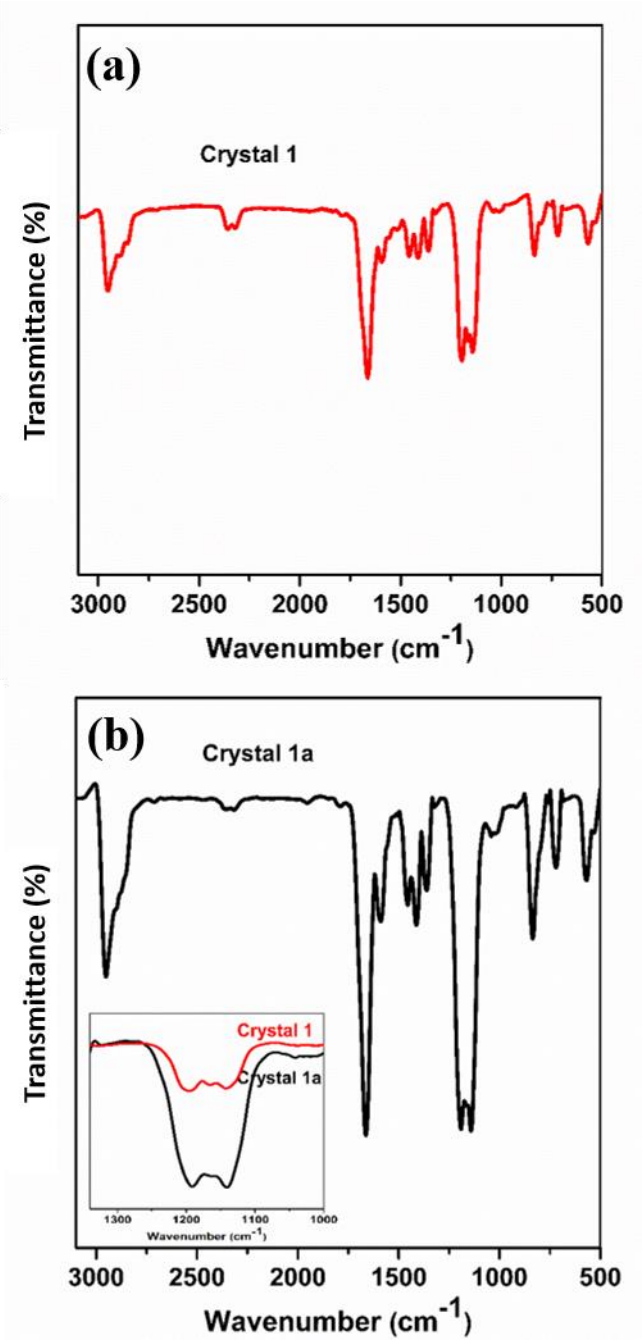

Fig. S22 (a) FT-IR spectra of **crystal 1**. The peaks between 2800 and 3000 cm^{-1} correspond to the ν_{C-H} stretching frequency of terminal *tert*-butyl groups of thiolate ligand, peaks at 1662 and 1587 cm^{-1} correspond to the $\nu_{C=O}$ stretching frequency of trifluoroacetate and ν_{C-N} stretching frequency from the linker molecules respectively (Fig. S5). The peaks at 1456 and 1357 cm^{-1} correspond to the ν_{C-H} bending vibrations and peaks at 1406 and 1193-1138 cm^{-1} correspond to the $\nu_{N=N}$ stretching vibration and ν_{C-F} stretching frequency, peaks at 837 and 725 cm^{-1} correspond to the $\nu_{C=C}$ stretching vibrations and peak at 569 cm^{-1} corresponds to the Ag-S stretching vibrations. (b) FT-IR spectra of **crystal 1a**, inset showing the peak-broadening in comparison with **crystal 1**.

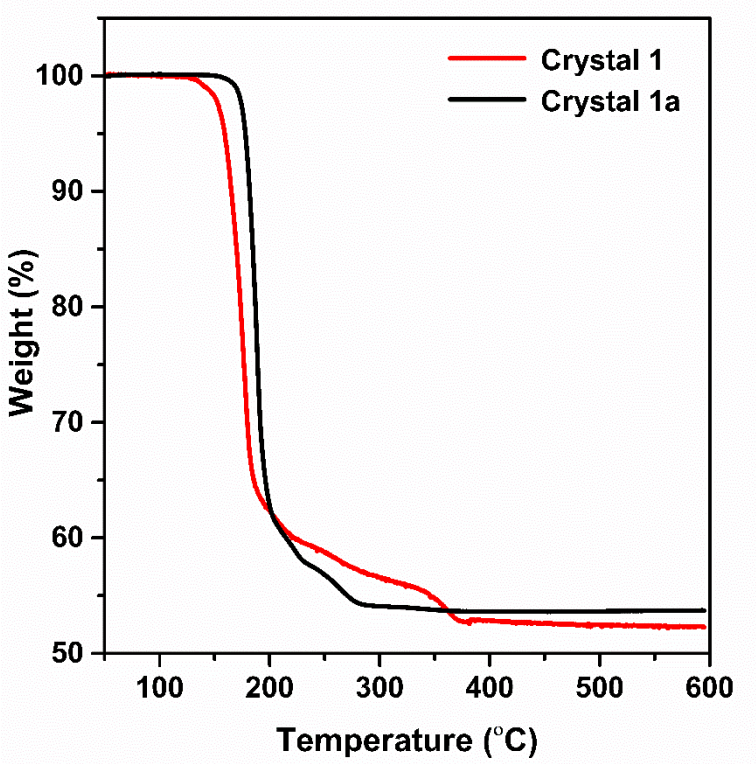

Fig. S23 TGA of both **crystal 1** and **crystal 1a**.

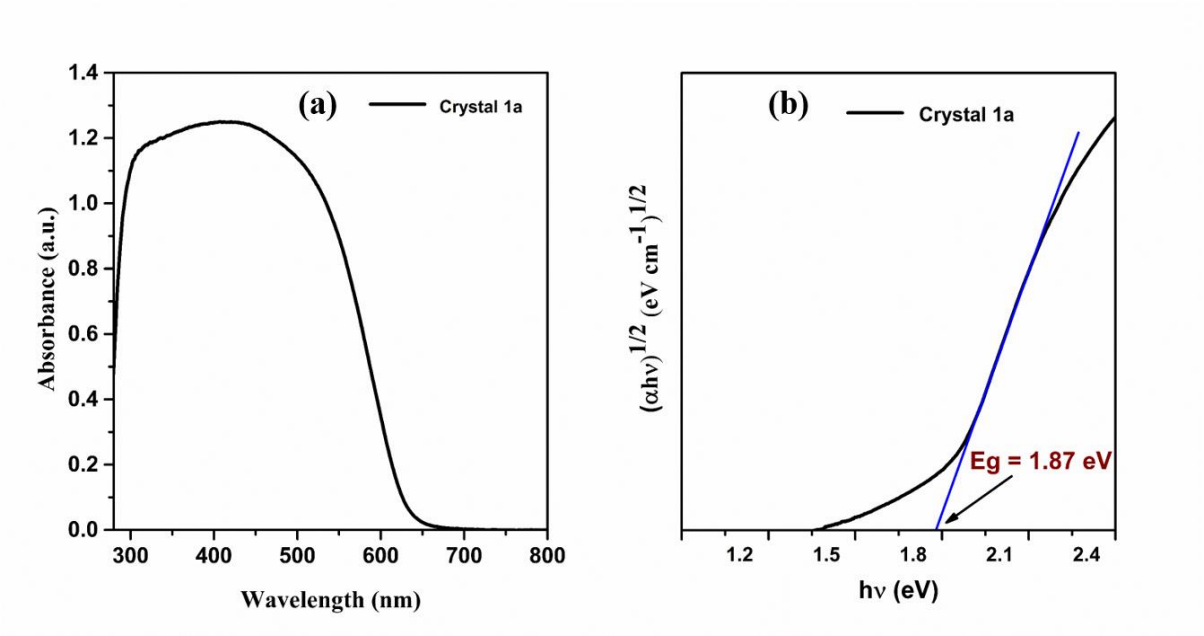

Fig. S24 (a) Solid-state UV-vis absorbance of **crystal 1a** and (b) its characteristic band gap energy.

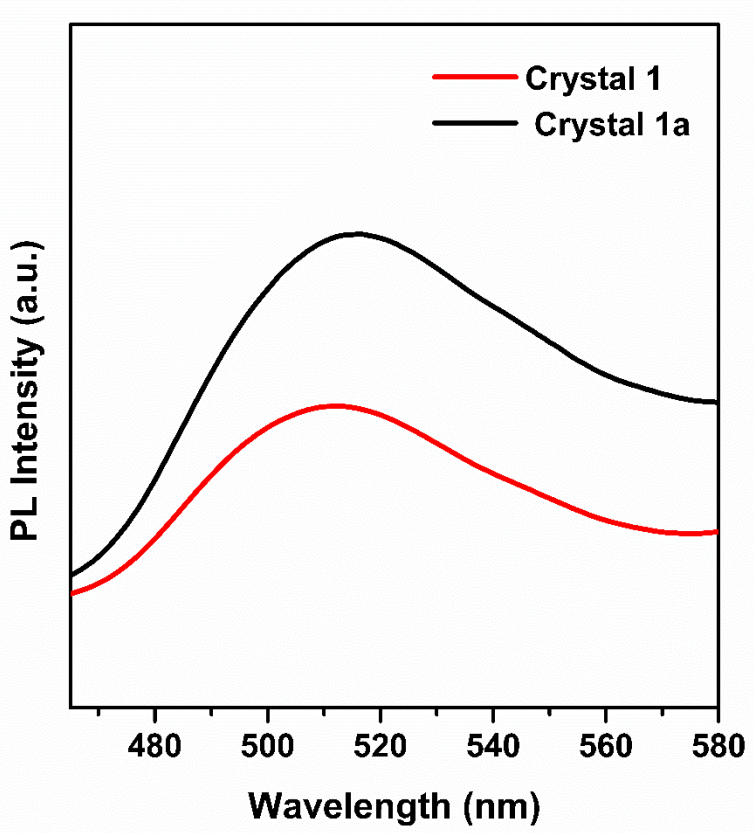

Fig. S25 Solid-state PL of both **crystal 1** and **crystal 1a**.

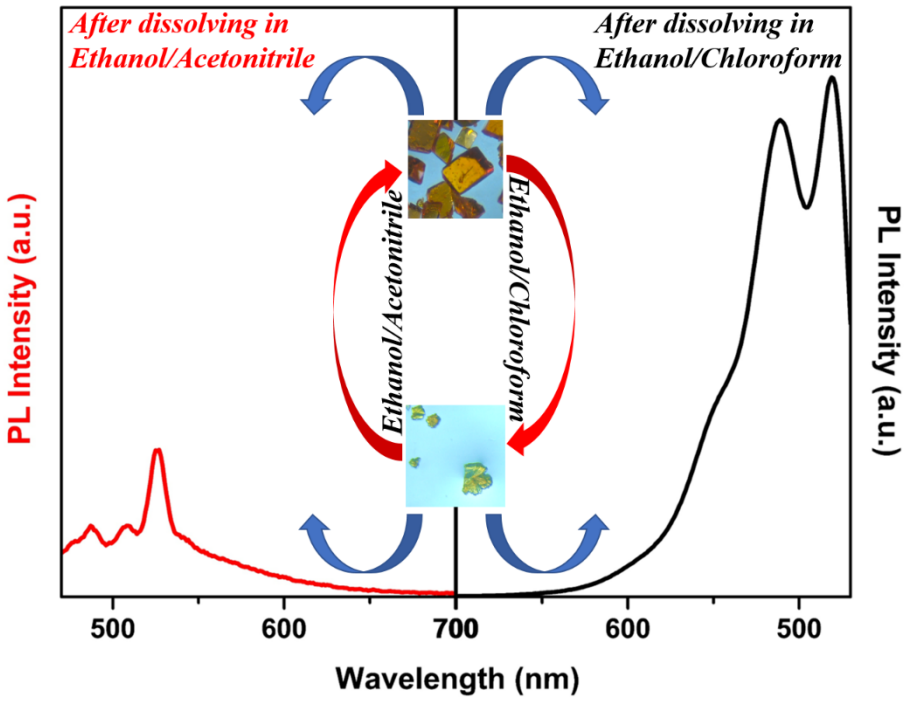

Fig. S26 Schematic representation of interchanging behavior of both **crystal 1** and **crystal 1a** in the different solvent mixture.

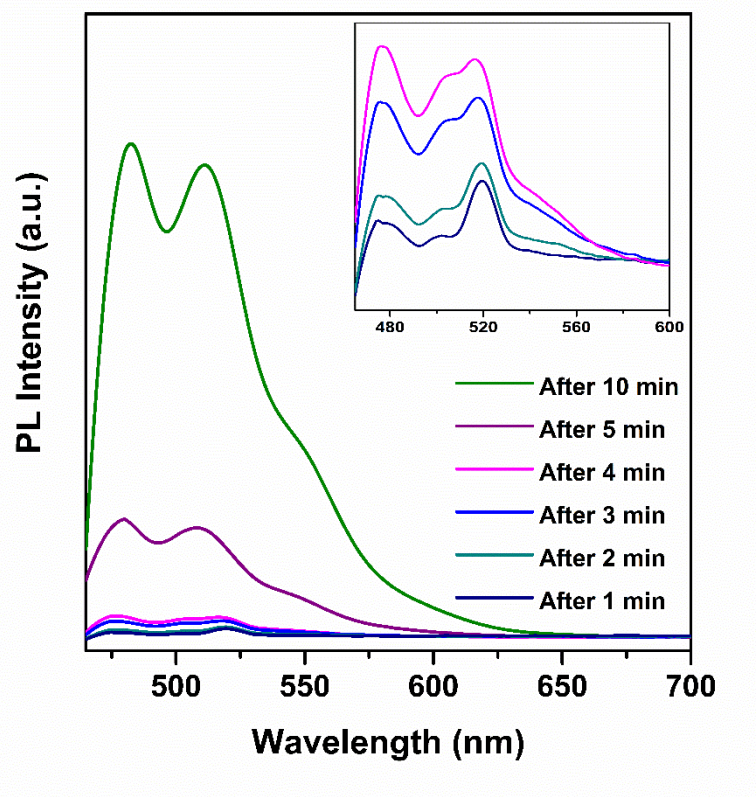

Fig. S27 Dynamics of **crystal 1** in E/C towards the highest PL intensity.

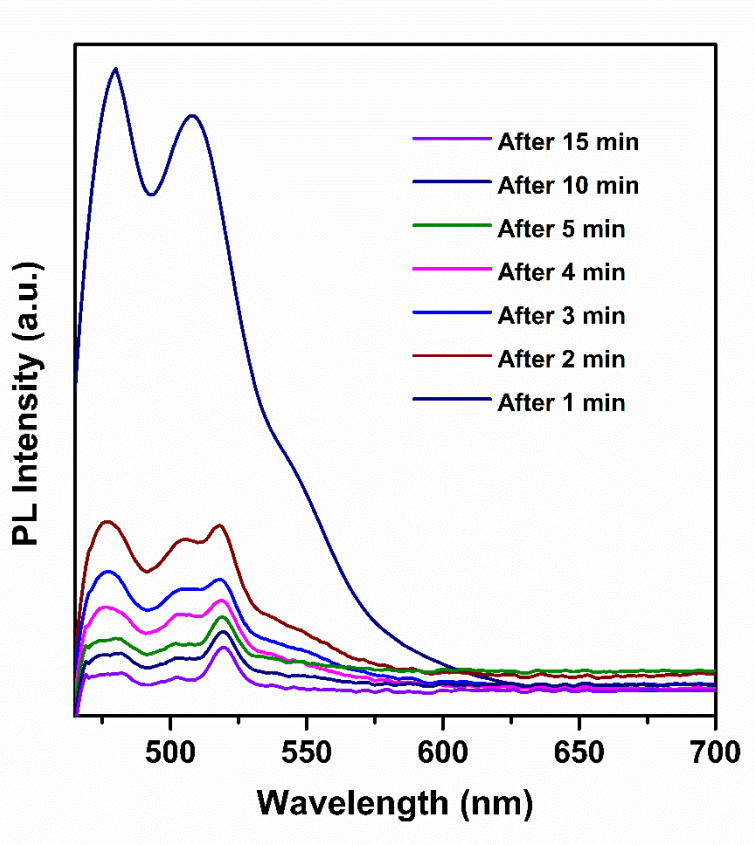

Fig. S28 Dynamics of **crystal 1a** in E/A towards the lowest PL intensity.

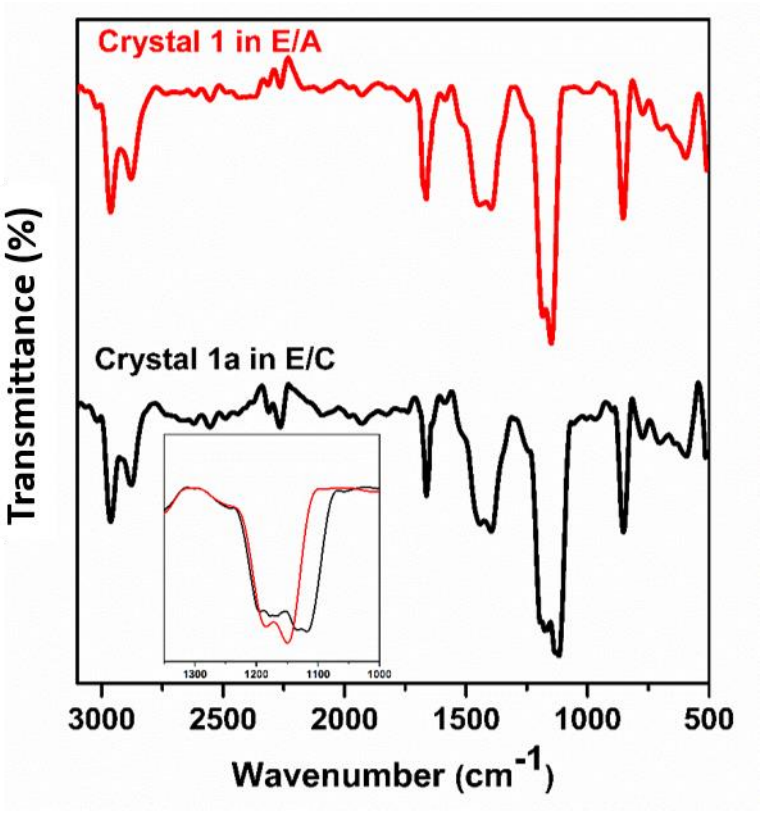

Fig. S29 FT-IR spectra of **crystal 1** and **crystal 1a** in their respective solvent mixtures.

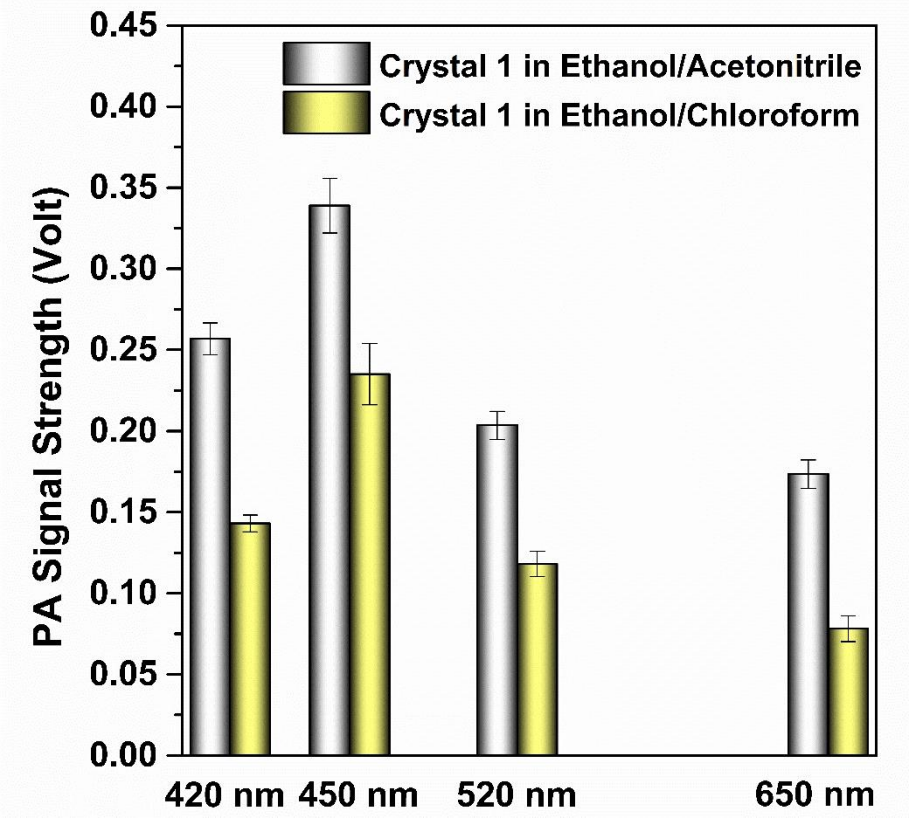

Fig. S30 PA signal strength of both solution of **crystal 1** at different wavelength.

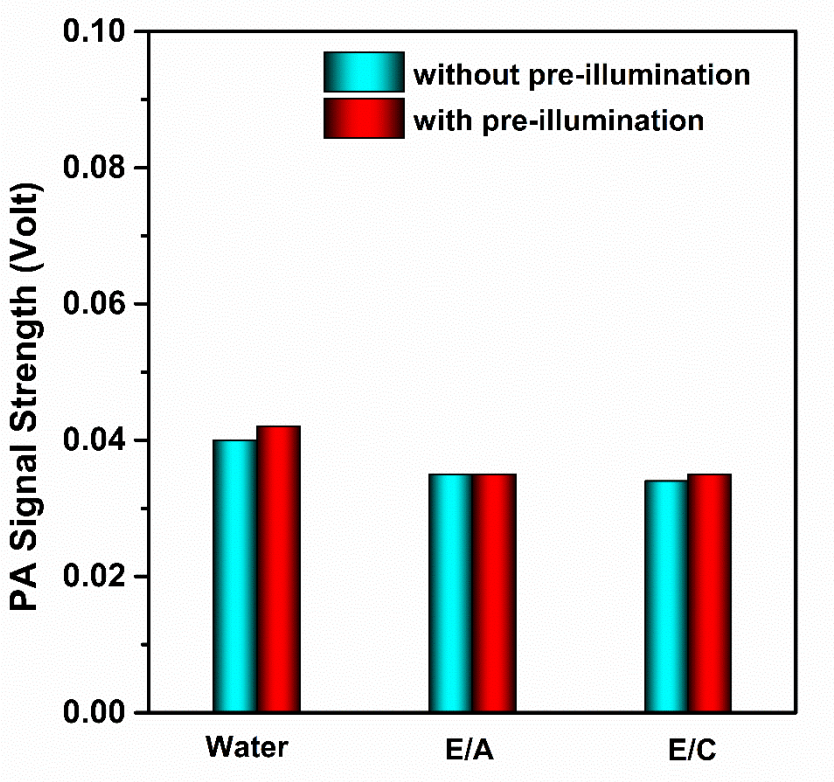

Fig. S31 PA signal strength of the solvents for control.

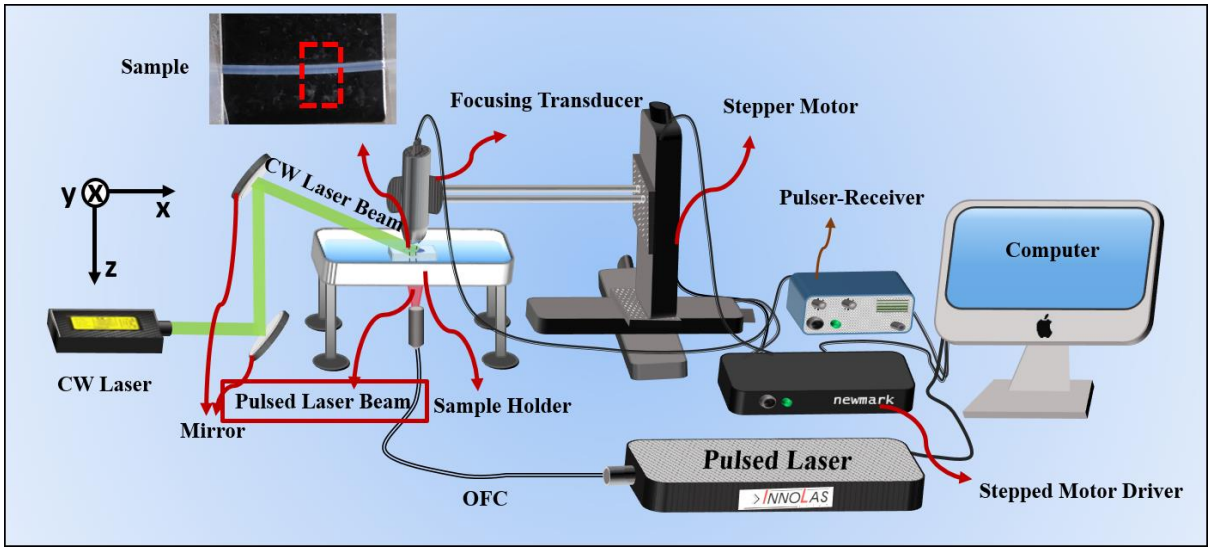

Fig. S32 Schematic representation of pre-illumination PA signal detection technique adapted in the AR-PAM imaging system. Inset depicts a typical (optical) photograph of the (plastic) tube being fixed in a base. During the experiments with the AR-PAM imaging system, the sample solution of interest (nanocluster, in our case) was introduced through the tube.

Reference

1 G. Li, Z. Lei and Q.-M. Wang, *J. Am. Chem. Soc.,* 2010, **132**, 17678-17679.

2 G. M. Sheldrick, *Acta Crystallogr., Sect. C: Struct. Chem.,* 2015, **71**, 3-8.

3 G. M. Sheldrick, *Acta Crystallogr., Sect. A: Found. Adv.,* 2015, **71**, 3-8.

4 L. J. Farrugia, *J. Appl. Crystallogr.,* 2012, **45**, 849-854.

5 O. V. Dolomanov, L. J. Bourhis, R. J. Gildea, J. A. Howard and H. Puschmann, *J. Appl. Crystallogr.,* 2009, **42**, 339-341.

6 M. J. Frisch, G. W. Trucks, H. B. Schlegel, G. E. Scuseria, M. A. Robb, J. R. Cheeseman, G. Scalmani, V. Barone, G. A. Petersson, H. Nakatsuji, X. Li, M. Caricato, A. V. Marenich, J. Bloino, B. G. Janesko, R. Gomperts, B. Mennucci, H. P. Hratchian, J. V. Ortiz, A. F. Izmaylov, J. L. Sonnenberg, Williams, F. Ding, F. Lipparini, F. Egidi, J. Goings, B. Peng, A. Petrone, T. Henderson, D. Ranasinghe, V. G. Zakrzewski, J. Gao, N. Rega, G. Zheng, W. Liang, M. Hada, M. Ehara, K. Toyota, R. Fukuda, J. Hasegawa, M. Ishida, T. Nakajima, Y. Honda, O. Kitao, H. Nakai, T. Vreven, K. Throssell, J. A. Montgomery Jr., J. E. Peralta, F. Ogliaro, M. J. Bearpark, J. J. Heyd, E. N. Brothers, K. N. Kudin, V. N. Staroverov, T. A. Keith, R. Kobayashi, J. Normand, K. Raghavachari, A. P. Rendell, J. C. Burant, S. S. Iyengar, J. Tomasi, M. Cossi, J. M. Millam, M. Klene, C. Adamo, R. Cammi, J. W. Ochterski, R. L. Martin, K. Morokuma, O. Farkas, J. B. Foresman and D. J. Fox, Wallingford, CT, 2016.

7 A. D. Becke, *J. Chem. Phys.,* 1993, **98**, 5648-5652.

8 P. J. Hay and W. R. Wadt, *J. Chem. Phys.,* 1985, **82**, 270-283.

9 W. R. Wadt and P. J. Hay, *J. Chem. Phys.,* 1985, **82**, 284-298.

10 V. Barone and M. Cossi, *J. Phys. Chem. A,* 1998, **102**, 1995-2001.

11 G. Kresse, J. Furthmüller and J. Hafner, *Phys. Rev. B,* 1994, **50**, 13181.

12 J. P. Perdew, J. A. Chevary, S. H. Vosko, K. A. Jackson, M. R. Pederson, D. J. Singh and C. Fiolhais, *Phys. Rev. B,* 1992, **46**, 6671.

13 G. Kresse and D. Joubert, *Phys. Rev. B,* 1999, **59**, 1758.

14 A. Thomas, S. Paul, J. Mitra and M. S. Singh, *Sensors,* 2021, **21**, 1190.